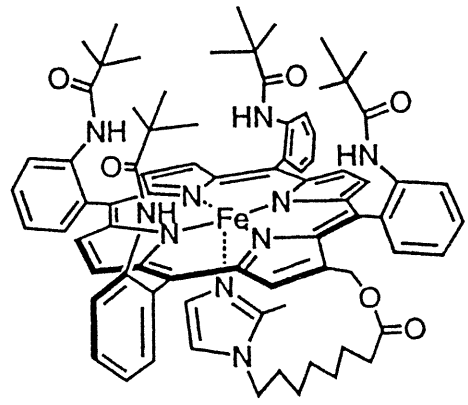

FeP1

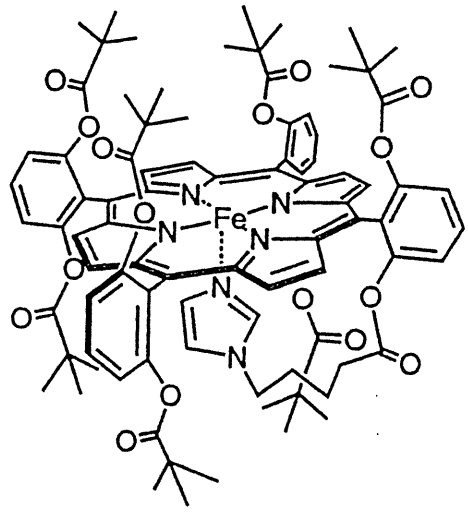

FeP2

Equilibrium constants for FeP binding to HSA.

Based on the quantitative analysis of the free FeP(CO) molecule in the solution prepared with different FeP/HSA mixing ratios (1-14), the equilibrium constants were determined using stepwise equilibrium models. We used the extraction procedure with chloroform to detect the free Fe(CO) amount in the solution [8]. After the evaporation of the organic phase, the residue was redissolved into methanol, and the FeP concentration was measured from the absorption spectra (ε_{max} at 417 nm: 2×10^5 $M^{-1}cm^{-1}$).

Binding sites of the FeP molecules in HSA.

The binding sites of FeP were estimated from the binding inhibition by other ligands which occupied the major association sites of HSA. Palmitic acid, protoporphyrin IX sodium salts instead of hemin, and phenol red instead of bilirubin were used as the inhibitors. The quantitative analysis of FeP was again performed using HSA incorporating each ligand (molar ratio: 1/1) at 25°C. The maximal binding numbers of FeP were decreased less than the mixing ratio, if the FeP molecule could not displace the inhibitor in competitive binding.

Determination of the half-lifetime of the oxygenated HSA-FeP.

A 3 mL portion of the HSA-FeP(CO) solution in a 1-cm quartz cuvette was irradiated by visible light (500 W halogen lamp) under an oxygen atmosphere, yielding the oxy state of HSA-FeP. During light irradiation, the cuvette was sometimes cooled in an ice-water bath to prevent excess heating. The conversion to the oxy state was confirmed by its absorption spectral change (λ_{max}) from 543 nm to 546 nm. The half-lifetime of the oxy state ($\tau_{1/2}$) was determined from a decrease in the absorption at 546 nm.

RESULTS AND DISCUSSION

Stability of HSA-FeP

The HSA-FeP(CO) solutions (FeP/HSA: 1-8) were prepared by mixing an organic solution of FeP(CO) (0.15 mM) with an aqueous solution of HSA (18.8 μM), followed by ultrafiltration and dialysis processes. The obtained red-colored suspension could be stored at 4°C for more than one month and be kept as a freeze-dried powder for at least three months. No difference was observed in the turbidity, the incorporation ratio of FeP, and the filter permeability of the solution before and after the freeze-drying processes. The carbonyl state of FeP in HSA was easily converted to the oxy state by the irradiation of visible light under an oxygen atmosphere.

Equilibrium constants of FeP binding to HSA

The albumin molecule is somewhat like a sponge. Based on an interest in the non-specific molecular binding aspect, albumin research involving binding studies has been widely developed [9]. Most ligands are bound reversibly with typical equilibrium constants (K) ranging from 10^6 to 10^4 M^{-1}. From the quantitative analyses of the free FeP1 molecule in the solution, the incorporation ratios were determined to be 100% for FeP1/HSA: 1, 99% for 4, 94% for 8, but only 60% for 14 (FIGURE 1). The concentration of HSA was always constant (5 wt%) independent of the mixing ratio. We concluded that the maximal binding ratio of FeP to one HSA molecule was eight. The binding data have mostly been

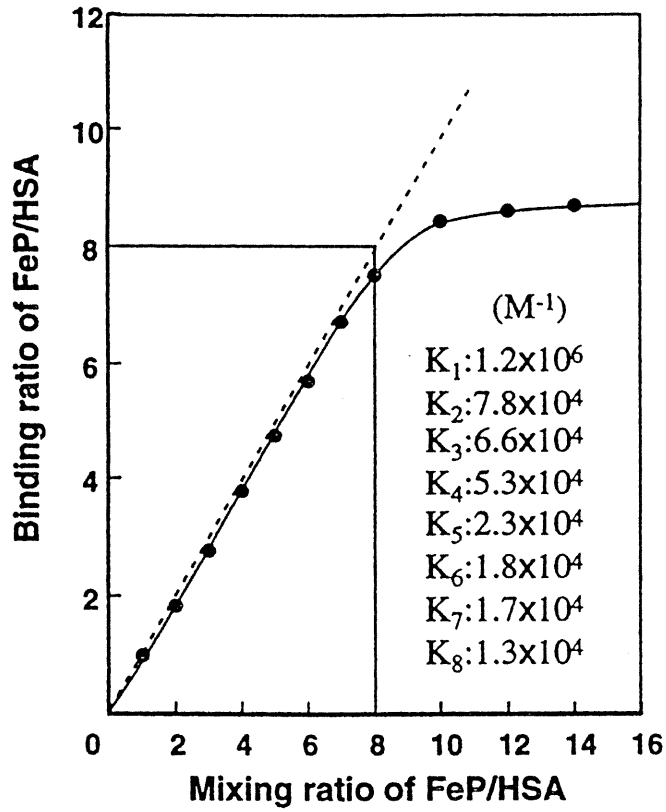

FIGURE 1 Relationship between mixing and binding ratios of FeP/HSA and stepwise equilibrium constants of FeP binding to HSA at 25°C.

analyzed according to the Scattchard model [1, 14]. We used, however, another means of analysis with a stepwise equilibrium model [15, 16]. The magnitude of the binding constants for the FeP association with HSA (K_1-K_8) ranged from $1.2x10^6$ to $1.3x10^4$ M^{-1}. These values are relatively low compared with those of palmitic acid (K_1-K_8: $6.2x10^7$-$3.8x10^5$ M^{-1}) and hemin (K_1: $5.0x10^7$ M^{-1}), which afford special interactions with albumin through their carboxylic groups. Preliminary results in circular dichroism measurement of HSA-FeP1 also suggests the weak binding of FeP with HSA [17]. Presumably the FeP molecule bind the host HSA only by hydrophobic interaction.

Binding sites of FeP in HSA molecule

According to the general consensus, there are six dominant regions of ligand association with albumin. The majority of the ligands are bound in one or both sites within specialized cavities of subdomains IIA and IIIA [10]. One or two fatty acids, for example, are absorbed by albumin under normal conditions [18]. There are, however, no clear conclusions about the exact location of bound

long-chain fatty acids. Crystallographic study of fatty acid binding to HSA is now being undertaken by Carter *et al.* On the other hand, it is almost accepted that bilirubin is primarily bound to a site within IIA. Concerning hemin, Hrkal *et al.* reported that the primary binding site is located in the sequence 124-298, which corresponds to subdomains Ib, IIa [19]. At a FeP/HSA mixing ratio of eight, the binding numbers are significantly decreased in all cases with inhibitor molecules (TABLE 1); one of the eight binding regions of FeP is obviously occupied by the inhibitor ligand. Consequently, the primary association sites of these ligands are one of the binding site of FeP. It is remarkable that the FeP binding was inhibited even by phenol red with a low K_I of 2.5×10^4 M^{-1}. This indicated that a minor binding site, at least a 5th one, of FeP was obviously blocked by phenol red.

Half-lifetime of O_2-coordinated FeP in HSA

The visible absorption spectral pattern of a deoxygenated double-sided heme (FeP2) bound HSA (HSA-FeP2; λ_{max}: 435, 537, 563 nm) shows a typical five-coordinated porphinatoiron(II) species, indicating that the covalently attached imidazolyl group was intramolecularly bound to the central iron. This spectrum changed to that of oxy type (λ_{max}: 423, 546 nm) upon the exposure to the air or oxygen. This O_2-association and dissociation are reversibly, and the degree of oxygenation corresponds to the O_2-partial pressure; O_2-binding affinity ($P_{1/2}(O_2)$) was 11 Torr at 37°C. The carbonyl state (λ_{max}: 425, 543 nm) was also immediately generated upon exposure to carbon monoxide gas with either the deoxy or oxy state.

The absorption band of the oxy state (546 nm) decreased slowly and almost disappeared after 24 hr, affording the completely oxidized hemin state. The half-lives ($\tau_{1/2}$) of the FeP2(O_2) were 15 hr at 25°C and 2.3 hr at 37°C, respectively (under 760 Torr O_2). Although the FeP molecules are incorporated into HSA by hydrophobic interaction, the micro-environments around FePs did not affect their O_2-binding behavior [8]. Autooxidation of the heme is therefore regulated only by its own hydrophobicity of the hemes around the O_2-binding site, *i.e.*, the pivalamide substituents on the porphyrin ring. In fact, the half-life of FeP2 with more hydrophobic groups was obviously longer than that of FeP1 (7 hr at 25°C, 1.2 hr at 37°C). It has been elucidated that the lifetime of O_2-binding to synthetic hemes and $P_{1/2}(O_2)$ in an organic solvent generally depend on their molecular structure and the properties of the solvent used, *e.g.*, polarity [20]. Especially in protic solvents, hydrophobic cavity around the central O_2-binding site is significantly effective to prevent an oxidation through proton driven process. Actually, the O_2-binding ability of the HSA-FeP system could be controllable by changing the molecular structure of the incorporated FeP. We are continuing the research on the tuning of the O_2-binding ability of this new oxygen-transport albumin.

TABLE 1 Binding numbers of FeP with HSA incorporating inhibitor ligands.

Inhibitors	FeP/HSA Mixing ratio 7	8	12
none	6.6	7.5	8.6
PPIX-Na_2	6.5	6.7	7.5
palmitic acid	6.5	6.7	7.6
phenol red	6.5	7.0	8.1

Moreover, there is much current interest in recombinant HSA (r-HSA) which has been recently manufactured by gene cloning [21]. The same results were obtained using r-HSA-FeP as a totally synthetic oxygen carrier. These compounds should act as new oxygen-carrying hemoprotein molecules instead of the hemoglobin in the blood stream.

ACKNOWLEDGMENT

This work was partially supported by the Core Research for Evolutional Science and Technology, JST and the Health Science Research Grants (Artificial Blood Project), the Ministry of Health and Welfare, Japan.

REFERENCES

1. Beaven GH, Chen S-H, D'Albis A, Gratzer WB: A Spectroscopic Study of the Haemin-Human-Serum-Albumin System. *Eur. J. Biochem.* **41**: 539-546 (1974).

2. Adams PA, Berman MC: Kinetics and Mechanism of the Interaction Between Human Serum Albumin and Monomeric Haemin. *Biochem. J.* **191**: 95-102 (1980).

3. Morgan WT, Smith A, Koskelo P: The Interaction of Human Serum Albumin and Hemopexin with Porphyrins. *Biochim. Biophys. Acta* **624**: 271-285 (1980).

4. Lamola AA, Asher I, Muller-Eberhard U, Poh-Fitzpatrick M: Fluorimetric Study of Binding of Protoporphyrin to Haemopexin and Albumin. *Biochem. J.* **196**: 693-698 (1981).

5. Marden MC, Hazard ES, Leclerc L, Gibson QH: Flash Photolysis of the Serum Albumin-Heme-CO Complex. *Biochemistry* **28**: 4422-4426 (1989).

6. Bonaventura J, Brouwer M, Brouwer T, Cashon B, Cameron S: presented in part at the 11th Congress ISABI, Boston, July, 1994.

7. Komatsu T, Ando K, Kawai N, Nishide H, Tsuchida E: O_2-Transport Albumin: A New Hybrid-Haemoprotein Incorporating Tetraphenyl-porphyrinatoiron(II) Derivative. *Chem. Lett.* **1995**: 813-814 (1995).

8. Tsuchida E, Ando K, Maejima H, Kawai N, Komatsu T, Tekeoka S, Nishide H: Properties of and Oxygen Binding by Albumin-Tetraphenylporphinatoiron(II) Derivative Complexes. *Bioconjugate Chem.* **8**: 534-538 (1997).

9. For example, Kragh-Hansen U: Molecular Aspect of Ligand Binding to Serum Albumin. *Pharmacological Reviews* **33**:17-53 (1981).

10. Carter DC, Ho JX: Structure of Serum Albumin. *Advanced in Protein Chemistry* **45**: 153-203 (1994).

11. He XM, Carter DC: Atomic Structure and Chemistry of Human Serum Albumin. *Nature* **356**: 209-215 (1992).

12. Tsuchida E, Komatsu T, Kumamoto S, Ando K, Nishide H: Synthesis and O_2-Binding Properties of Tetraphenylporphyrinato-iron(II) Derivatives Bearing a Proximal Imidazole Covalently Bound at the ß-pyrrolic Position. *J. Chem. Soc., Perkin Trans. 2* **1995**: 747-753 (1995).

13. Tsuchida E, Komatsu T, Arai K, Nishide H: Synthesis and Dioxygen-binding Properties of Double-sided Porphyrinatoiron(II) Complexes Bearing Covalently Bound Axial Imidazole. *J. Chem. Soc., Dalton Trans.* **1993**: 2465-2469 (1993).

14. Halfman CJ, Nishida T: Method for Measuring the Binding of Small Molecules to Proteins from Binding-induced Altercations of Physical-Chemical Properties. *Biochemistry* **11**: 3493-3498 (1972).

15. Fletcher JE, Sector AA, Ashbrook JD: Analysis of Macromolecule-Ligand Binding by Determination of Stepwise Equilibrium Constants. *Biochemistry* **9**: 4580-4587 (1970).

16. Ashbrook JD, Sector AA: Santos EC, Fletcher JE: Long Chain Fatty Acid Binding to Human Plasma Albumin. *J. Biological Chem.* **250**: 2333-2338 (1975).

17. Komatsu T, Tsuchida E, *et al.,* manuscript in preparation.

18. Peter T Jr., Adv. *Protein Chem.* **37**: 161-245 (1985).

19. Hrkal Z, Klementova S: Bilirubin and Haeme Binding to Human Serum Albumin Studied by Spectroscopy Methods. *J. Biochem.* **16**: 799-804 (1984).

20. Momenteau M, Reed CA: Synthetic Heme Dioxygen Complexes. *Chem. Rev.* **94**: 659-698 (1994).

21. Sumi A, Ohtani W, Kobayashi K, Ohmura T, Yokoyama K, Nishida M, Suyama T: Purification and Physicochemical Properties of Recombinant Human Serum Albumin. *Biotechnology of Blood Proteins* ed. Rivat C, Stolts JF, Vol. 227, pp 293-298, John Libbey Eurotext Ltd. (1993).

原著

リコンビナントアルブミンーヘム複合体の物性と酸素結合能

小松晃之，浜松和芳，松川泰子，呉　健，土田英俊*

Dioxygen-binding Ability of Recombinant Albumin-heme Hybrid

Teruyuki Komatsu, Kazuyoshi Hamamatsu, Yasuko Matsukawa,
Jian Wu, Eishun Tsuchida*

リコンビナントヒト血清アルブミン(rHSA)にテトラフェニルポルフィリン鉄(II)誘導体(FeP)を包接させて得たリコンビナントアルブミンーヘム複合体(rHSA-FeP)が，生理的条件下(pH 7.4, 37°C)で酸素を可逆的に結合解離できる新しい合成ヘム蛋白質となることを実証した．FePはrHSA当たり最大8分子まで導入できる．rHSA-FeP溶液([rHSA]: 5g/dL)の粘度，膠質浸透圧，等電点，及びrHSAの二次構造はFePの結合数によらず一定であった．ヒト全血液と混合した場合でも凝集の惹起はなく，血液適合性も高い．酸素の通気に伴い速やかに酸素錯体を形成し，その酸素配位構造を共鳴ラマンスペクトル測定(ν(Fe-O_2): 560 cm^{-1})から確認した．また，酸素親和性($P_{1/2}$: 33 Torr, n: 1.0)，酸素結合解離速度定数(k_{on}: 2.5x10^7 ($M^{-1}s^{-1}$)，k_{off}: 5.6x10^2 (s^{-1}))を決定し，rHSA-FeP溶液が人工酸素輸液(赤血球代替物)としての機能を有することを明らかにした．

Incorporation of tetraphenylporphyrinato-iron(II) derivatives (FeP) into recombinant human serum albumin (rHSA) provides a new type of artificial hemoprotein (rHSA-FeP), that binds and releases dioxygen reversibly under physiological conditions (in aqueous media, pH 7.4, 37°C). The rHSA host adsorbs a maximal eight FeP molecules. The viscosity, colloid osmotic pressure, surface charge distribution, and second-order structure of the rHSA-FeP hybrid ([rHSA]: 5 g/dL, FeP/HSA = 1~8 (mol/mol)) are constant and independent of the binding numbers of FePs. Furthermore, the obtained solution showed good blood compatibility. The O_2-coordination structure of FeP embedded into certain hydrophobic domains of the albumin was confirmed by resonance Raman spectroscopy (ν(Fe-O_2): 560 cm^{-1}). The O_2-binding affinity ($P_{1/2}$: 33 Torr, n: 1.0) and O_2-association and -dissociation rate constants (k_{on}: 2.5x10^7 ($M^{-1}s^{-1}$), k_{off}: 5.6x10^2 (s^{-1})) are also determined. These results show that rHSA-FeP hybrid has an ability to act as synthetic O_2-infusion (red cell substitute). —Key Words: Tetraphenylporphyrinato-iron(II) derivative, Recombinant human serum albumin, Heme, Dioxygen-binding, Artificial hemoprotein, O_2-infusion, Blood substitute.

1. 緒言

ヒト血清アルブミン(HSA，Mw: 66.5 kD)は血漿蛋白質の約60%を占め，血液の膠質浸透圧維持のほか，種々の薬物または代謝産物を非特異的に結合し体内の目的箇所へ運搬する輸送蛋白質としての役割を果たしている[1,2]．この非特異的多分子結合能への関心は，永年に亘ってHSAの分子包接に関する研究を促進してきた[3,4]．また，1989年にはHSAのX線結晶構造が解明され，ついにその立体構造の全容が明らかにされた[5-7]．HSAは従来考えられていた長楕円型ではなく，正三角形に近いハート型(幅: 8 nm, 深さ: 3 nm)であった．9個のループと17個のジスルフィド結合から構成される3つのドメイン(I～III)からなり，さらにその各々は2つのサブドメイン(A, B)に分けられる．ヘモグロビンから遊離したヘミン(プロトポルフィリン鉄(III)錯体)はサブドメインIB～IIAに結合し肝臓に運ばれる．結合定数(K_1)は10^6～10^9 (M^{-1})と報告されており[8-10]，いわゆるポルフィリン鉄を含有するヘム蛋白質系を構成するが，従来このアルブミンーヘミン複合体の機能応用について検討された例はほとんどなかった[11]．我々は，独自に分子設計・合成した軸塩基(イミダゾリル基)を有するテトラフェニルポルフィリン鉄(II)誘導体(FeP，Fig. 1)をHSAの疎水ドメインへ包接させると，安定なヘム複合体(アルブミンーヘム(HSA-FeP))が得られることを明らかにしている[12,13]．FePの結合サイトは，サブドメインIB, IIA, IIIB他が推定されており，HSA当たり最大8分子までのFePが包接される[14]．さらにこの合成ヘム蛋白質は，ヘモグロビンやミオグロビンと同様に生理的条件下(pH 7.4, 37°C)で酸素分

*To whom correspondence should be addressed.
早稲田大学理工学総合研究センター高分子化学研究室，〒169-8555 東京都新宿区大久保3-4-1, Department of Polymer Chemistry, Advanced Research Institute for Sci & Eng, Waseda University, 3-4-1 Okubo, Shinjuku, Tokyo 169-8555, Japan.
論文受付98年11月5日，受理98年11月26日．

子を可逆的に結合解離することができるので，赤血球代替物としての利用が期待されており，現在その機能評価が進められている．

また近年，ピキア酵母(*Pichia pastoris*)によるリコンビナントヒト血清アルブミン(rHSA)の大量産生技術が確立された[15]．構造，アミノ酸配列，物理化学的特徴はHSAと完全に一致しており，HSA代替製剤としての供給を目指して2000年の上市が予定されている．我々はごく最近，このrHSAにFePを包接させたいわゆる完全合成型のヘム蛋白質，リコンビナントアルブミンーヘム複合体(rHSA-FeP)を新たに作製し，この溶液が人工酸素輸液としての充分な機能を具有することを実証した．本報文では，rHSA-FeP複合体の物理化学的特徴と酸素結合パラメータについて報告する．

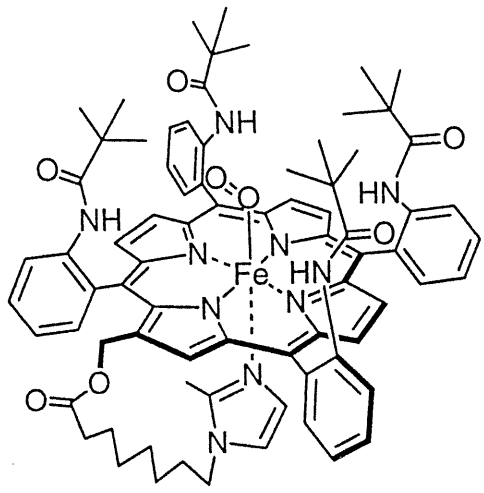

Fig. 1 Tetraphenylporphyrinato-iron(II) derivative with a covalently bound axial imidazole (FeP).

2. 実験方法

2.1 rHSA-FeP溶液の調製

FePは著者らの前報文に従い合成し[16]，rHSA(25 g/dL (3.75 mM))は吉富製薬社製を使用した．FePのエタノール溶液([FeP]: 0.15 mM)にCO下でアスコルビン酸(AsA)水溶液を添加(AsA/FeP: 1 mol/mol)すると，中心鉄がFe(II)に還元されFeP(CO)体が得られる．これをrHSAのリン酸生理緩衝溶液(10 mM, pH 7.3, [rHSA]: 18.8μM)に滴下混合し，すぐにエタノールを減圧除去する．限外ろ過(限外分子量: 5万，圧力: 4 kg/cm^2)，透析(透析膜: 分画分子量12,000～14,000，再生セルロース)により，エタノール，酸化型デヒドロアスコルビン酸を除外し，赤色透明のrHSA-FeP(CO)溶液([rHSA]: 5 g/dL (5 wt%))を得た．異なるFeP結合比(FeP/HSA: 1, 4, 8 (mol/mol))の試料を調製し，測定に供した．得られたrHSA-FeP(CO)を酸素通気下で光照射(500W ハロゲンランプ，5 min)すると，COが脱離しその可視吸収スペクトルはoxy型となる．さらにそこへ窒素を通気すると可視吸収スペクトルはdeoxy型へ移行し，酸素の吹き込みに伴い再びoxy型へ戻った．

HSAの定量はブロモクレゾールグリーンによる色素定量法(アルブミン-テストワコー，和光純薬)により行った．

2.2 物理化学測定

等電点電気泳動はPhastsystem (Pharmacia)，CDスペクトルは円二色性分光計J-720W (JASCO)を用いて測定した[14]．rHSA-FeP(5g/dL)のコロイド浸透圧，及び粘度は，各々コロイド浸透圧計 4420 COLLOID OSMOMETER (WESCOR)，キャピラリー粘度計 DCS300 (Anton Paar)を用いて決定した[14]．ヒト全血液はEDTAを含む採血管で採取し，同量のrHSA-FeP溶液と混合した後，すぐに粘度測定に供した．また，共鳴ラマンスペクトルは共鳴ラマン分光光度計 NRS-2000 (JASCO)を用い，oxy体，deoxy体について測定した(励起波長: 457.9 nm (Ar^+ イオンレーザー))[14]．

2.3 酸素親和性，及び酸素結合解離速度定数の測定

rHSA-FeP溶液([FeP]: 15μM)に異なる酸素分圧の酸素／窒素混合ガスを吹き込み，その時の可視吸収スペクトル変化から，酸素親和性($P_{1/2}$)を決定した．酸素結合反応の熱力学パラメータ(ΔH, ΔS)は van't Hoffプロットから算出し，酸素の結合解離速度定数(k_{on}, k_{off})はレーザーフラッシュフォトリシス分光装置TSP-601 (UNISOKU)を用いて決定した[13]．酸素錯体半減期($\tau_{1/2}$)はoxy体(552 nm)の吸光度の経時変化から算出した．

3. 結果および考察

赤色のrHSA-FeP([rHSA]: 5 g/dL)は調製6ヵ月後(4°C保存)でも沈殿や凝集は認められず，きわめて安定な溶液である．可視吸収スペクトルにおける427 nmの吸光度とFeP分子のモル吸光係数から，rHSAには最大8分子までのFePが導入できることを明らかにした．これは従来のHSA-FeP系の場合と同様であり，FePの逐次平衡定数は K_1: 10^6 (M^{-1})～K_8: 10^4 (M^{-1})程度と考えられる[14]．

一般にアルブミンへ界面活性剤などが結合した場合，高次構造変化が誘発される[17]．しかし，rHSA-FePのCDスペクトルパターン，及びその強度はrHSA単独の場合と同様で，$[\theta]_{208}$の値から算出したα-helix含量[18]も約60%であった．また，結合したFePによる誘起CD[19]が400 nm付近に観測されなかったことから，rHSAへのFeP分子の取り込みは疎水性相互作用のみによるものと推定される．

rHSA-FePの等電点(pI)，コロイド浸透圧は，FePの結合比(1～8)に関わらず4.8(Fig. 2)，18 mmHg([rHSA]: 5 g/dL)であり，rHSAの値と同等であった．すなわちFePの結合に伴う表面電荷の変化はなく，これはアルブミン自身の本来有する特性(膠質浸透圧調整や血漿増量作用)が損われないことを意味する．さらに，rHSA-FeP溶液の粘度曲線はニュートン性であり，測定ずり速度範囲(0～350 s^{-1})内にて一定の低粘度(1.1 cP)を示した(Fig. 3)．ヒト全血液と混合しても凝集や沈殿の惹起は見られなかった．さらに混合溶液を光学顕微鏡で観察したが，赤血球の形状に全く変化はなく，高い血液適合性が明らかとなった(Fig. 4)．

rHSA-FePのdeoxy体溶液に酸素を通気すると，可視吸収スペクトル(λ_{max}:443, 542, 567 nm) は 速やかにoxy体のスペクトル(λ_{max}: 426, 552 nm)へ移行し，その酸素結合解離は可逆的であった(Fig. 5)．続いて一酸化炭素を通気すると安定なcarbonyl体(λ_{max}:427, 539 nm)を形成した．酸素錯体の半減期($\tau_{1/2}$)は，8hr(25°C)，2hr

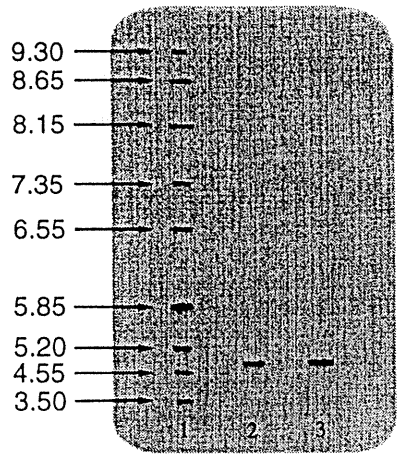

Fig. 2 IEF patterns of rHSA and rHSA-FeP. Lane 1: markers, lane 2: HSA, lane 3: HSA-FeP (8) from the left.

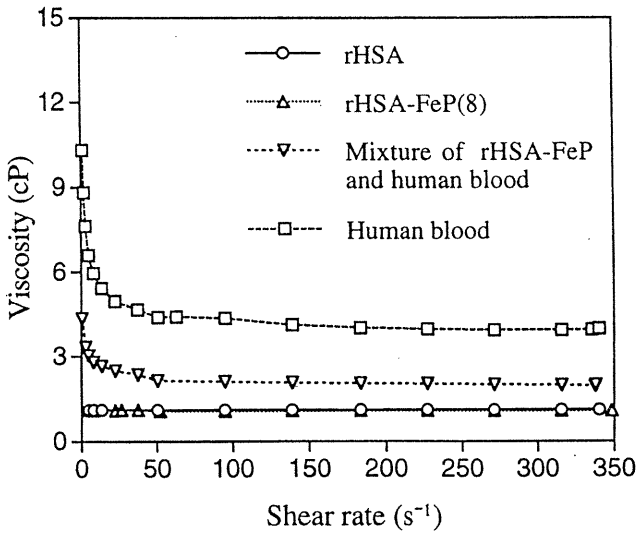

Fig. 3 Change in the viscosity of rHSA-FeP at various shear rates.

(37°C)であり，従来のHSA-FeP系と同等であった[14]．この$\tau_{1/2}$の値については，*in vivo* で大きく延長するという興味ある結果も得ている[20]．

次いで，共鳴ラマンスペクトル測定から，FePの配位構造，配位酸素の電子状態を確認した(Fig. 6)．deoxy型のスペクトルに見られる198 cm^{-1}のピークは，イミダゾール基が分子内配位した5配位高スピンFe(II)錯体のν(Fe-Nε)に相当する[21]．酸素の通気に伴い，新たにν(Fe-O_2)由来の吸収が560 cm^{-1}に出現したことから，酸素配位錯体の形成が明らかとなった．これはヘモグロビンやミオグロビンで観測される値と類似しており，酸素分子がいわゆるend-on型で中心鉄に結合している構造を示唆する[22,23]．さらに，

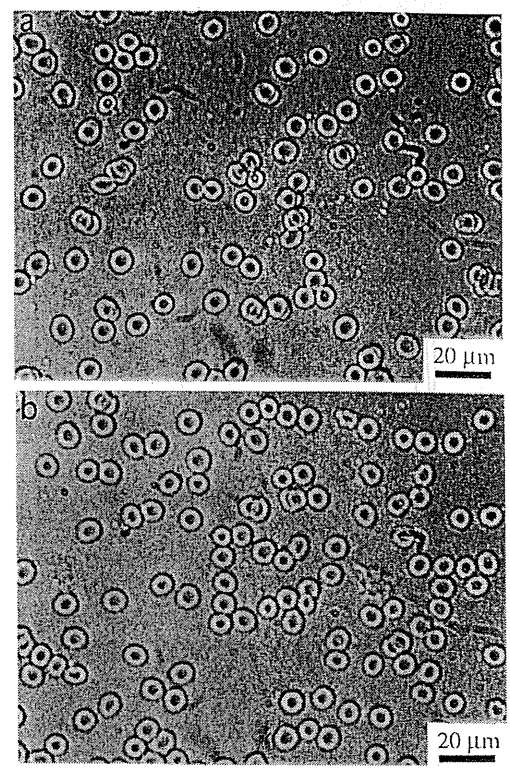

Fig. 4 Optical microscopic observation of (a) rHSA + human whole blood and (b) rHSA-FeP(8) + human whole blood.

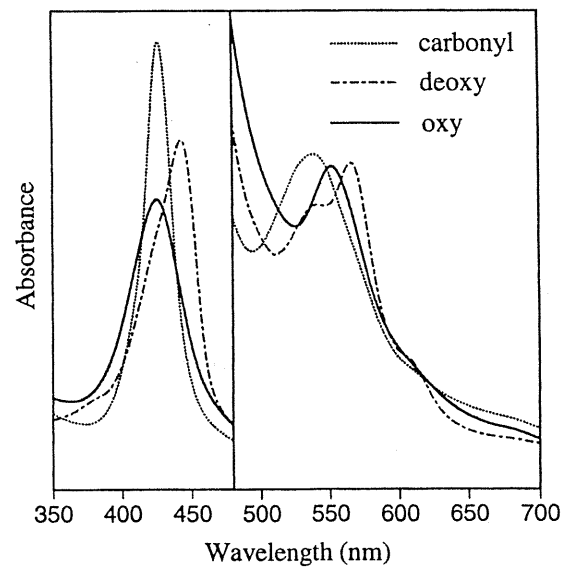

Fig. 5 Visible absorption spectral changes of rHSA-FeP in phosphate buffer (pH 7.4) at 25°C.

ポルフィリン環に基づく高強度の伸縮振動(ν_4, ν_8)[21,24]も各々1346, 370cm^{-1}(窒素雰囲気下)から, 1364, 394cm^{-1}(酸素雰囲気下)に移行し, deoxy体からoxy体への変換を示した.

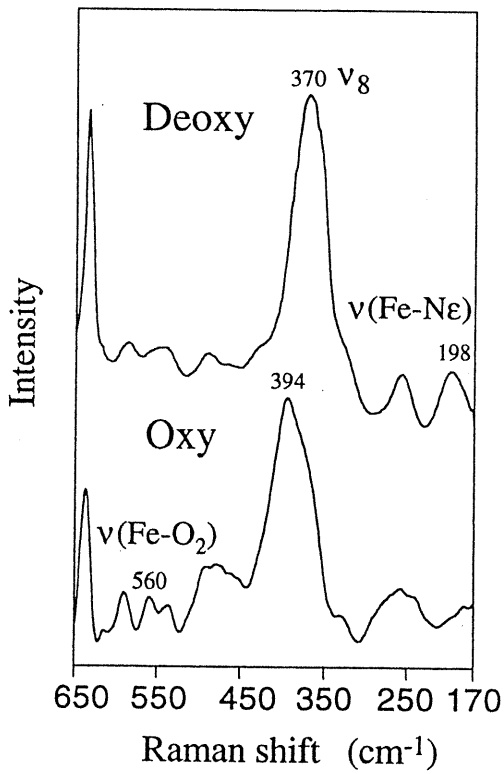

Fig. 6 Resonance Raman spectra of rHSA-FeP solution at 25°C.

rHSA-FePの酸素結合解離曲線(Fig. 7)から酸素親和性を算出した($P_{1/2}$: 33～37Torr). ヘモグロビンのような酸素結合の協同効果は見られない(Hill係数は1.0)が, 肺(Po_2: 110Torr)－末梢組織(Po_2: 40Torr)間における酸素運搬効率は22%で, 赤血球の値(23%)に匹敵する充分な酸素輸送能力を有する. また, rHSA-FePの酸素結合における熱力学パラメータ(ΔH, ΔS)は, 各々-61 kJ / mol, -114 J/K・molで, ヘモグロビンの値と同等であった(Table 1).

Table 1 O_2-binding parameters of rHSA-FeP at 25℃

	$P_{1/2}$[1] (Torr)	$10^{-7}k_{on}$ ($M^{-1}s^{-1}$)	$10^{-2}k_{off}$ (s^{-1})	ΔH (kJ/mol)	ΔS (J/K·mol)
rHSA-FeP(4)	13 (37)	1.9	4.3	-61	-114
rHSA-FeP(8)	13 (33)	2.5	5.6	-61	-115
Red blood cell	9 (27)	0.0011	0.0016	—	—
Hb(T-state)α	40	0.29	1.8	-57 － -65	-116 － -113

[1] at 37℃ in parenthesis.

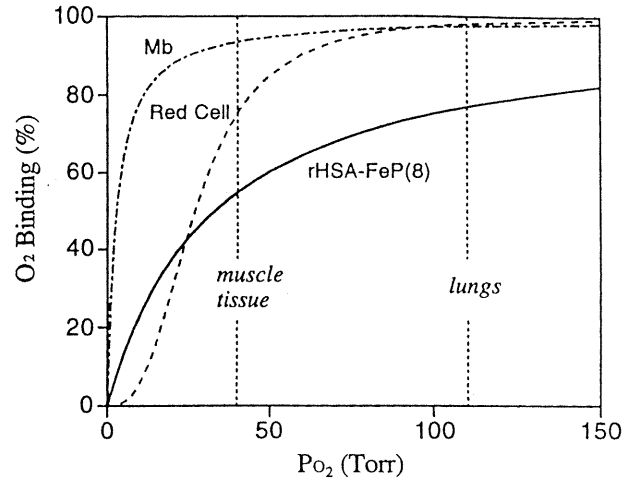

Fig. 7 O_2-binding equilibrium curve of rHSA-FeP(8) at 37°C.

レーザーフラッシュフォトリシス法から決定したrHSA-FePの酸素結合解離速度定数(k_{on}, k_{off})は血液の値よりも10^3倍大きく, 酸素を迅速に吸脱着できることが明らかとなった(Table 1). これらの結果から, rHSA-FePはヘモグロビンと同じ機構で酸素分子を結合しており, 完全合成型酸素輸液としての必要条件を兼ね備えていると考えられる. 現在 *in vivo* 酸素輸送能の評価が行われているほか, より高濃度の酸素輸送を目指して多量化アルブミン－ヘム系の合成も進行している.

4. 結語

FePはrHSAに最大8分子まで包接され、得られたrHSA-FeP複合体の溶液物性はrHSA自身と変わらない. これはFePのrHSAへの結合が疎水性相互作用によるためと考えられる. rHSA-FeP溶液は高い血液適合性を示し、生理的条件下で可逆的に酸素を結合解離できる. 酸素配位構造はヘモグロビンやミオグロビンと同じend-on型であると推定された. 酸素結合パラメータ, 酸素輸送効率は赤血球と比較して遜色なく, rHSA-FePが酸素輸液としての機能を具有することを実証した.

謝辞

本研究の一部は厚生科学研究費補助金(高度先端医療研究事業(人工赤血球))により行われた. 記して謝意を表する.

参考文献

1. Peters Jr T. All about albumin. Biochemistry genetics and medical applications. New York: Academic Press, 1996.
2. Brown JR. Serum albumin: amino acid sequence. In:Rosenoer VM, Oratz M, Rothschild MA, eds. Albumin structure, function and uses. New York: Pergamon Press, 1976;27-51.
3. Kragh-Hansen U. Molecular aspects of ligand binding to serum albumin. Pharmacological Reviews 1981;33:17-53.
4. Peters Jr T. Serum albumin. Adv Protein Chem 1985;37:161-245.
5. Carter DC, He X-M, Munson SH, Twigg PD, Gernert KM, Broom

MB, Miller TY. Three-dimensional structure of human serum albumin. Science 1989;244:1195-8.
6. He X-M, Carter DC. Atomic structure and chemistry of human serum albumin. Nature 1992;356:209-15.
7. Carter DC, Ho JX. Structure of serum albumin. Adv Protein Chem 1994;45:153-204.
8. Beaven GH, Chen S-H, D'Albis A, Gratzer WB. A spectroscopic study of the haemin-human-serum-albumin system. Eur J Biochem 1974;41:539-46.
9. Muller-Eberhand U, Morgan WT. Porphyrin-binding proteins in plasma. Ann NY Acad Sci 1975;244:625-50.
10. Adams PA, Berman MC. Kinetics and mechanism of the interaction between human serum albumin and monomeric haemin. Biochem J 1980;191:95-102.
11. Bonaventura J, Brouwer M, Brouwer T, Cashon B, Caneron S. presented in part at the 11th congress ISABI, Boston, July 1994.
12. Komatsu T, Ando K, Kawai N, Nishide H, Tsuchida E. O_2-transport albumin: a new hybrid-haemoprotein incorporating tetraphenylporphinatoiron(II) derivative. Chem Lett 1995;1995: 813-4.
13. Tsuchida E, Ando K, Maejima H, Kawai N, Komatsu T, Takeoka S, Nishide H. Properties of and oxygen binding by albumin-tetraphenylporphyrinatoiron(II) derivative complexes. Bioconjugate Chem 1997;8:534-8.
14. Komatsu T, Hamamatsu K, Matsukawa Y, Wu J, Tsuchida E. Physicochemical properties and O_2-coordination structure of human serum albumin incorporating tetrakis(*o*-pivalamido) phenylporphyrinatoiron(II) derivatives. Bioconjugate Chem 1998; 9: in press.
15. Sumi A, Ohtani W, Kobayashi K, Ohmura T, Yokoyama K, Nishida M, Suyama T. Purification and physicochemical properties of recombinant human serum albumin. In:Rivat J, Stolts JF, eds. Biotechnology of Blood Proteins. Montrouge:John Libbey Eurotext, 1993;227:293-8.
16. Komatsu T, Kumamoto S, Ando K, Nishide H, Tsuchida E. Synthesis and O_2-binding properties of tetraphenylporphyrinatoiron (II) derivatives bearing proximal imidazole covalently bound at the β-pyrrolic position. J Chem Soc Perkin Trans 2 1995;1995:747-53.
17. Aoki K, Okabayashi H, Maezawa S, Mizuno T, Murata M, Hiramatsu K. Raman studies of bovine serum albumin-ionic detergent complexes and conformational change of albumin molecule induced by detergent binding. Biochim Biophys Acta 1982;703:11-16.
18. Greenfield N, Fasman GD, Computed circular dichroism spectra for the evaluation of protein conformation. Biochemistry 1969;8:4108-16.
19. Casella L, Gullotti M, Poli S, DeGioia L. Heam-protein interactions. The binding of heam complexes to serum albumin. Gazzetta Chimica Italiana 1993;123:149-54
20. Komatsu T, Matsukawa Y, Tsuchida E. unpublished data.
21. Hori H, Kitagawa T. Iron-ligand stretching band in the resonance Raman spectra of ferrous iron porphyrin derivatives. Importance as a probe band for quaternary structure of hemoglobin. J Am Chem Soc 1980;102:3608-13.
22. Wu J, Komatsu T, Tsuchida E. Resonance Raman studies of dioxygen binding to *ortho*-substituted tetraphenyl- and tetranaphthyl-porphyrinatoiron(II) derivatives with a covalently linked axial imidazole. J Chem Soc Dalton Trans 1998;1998: 2503-6.
23. Hirota S, Li T, Philips Jr GN, Olson JS, Mukai M, Kitagawa T. Pertubation of the Fe-O_2 bond by nearby residues in heme pocket: observation of vFe-O_2 Raman bands for oxymyoglobin mutants. J Am Chem Soc 1996;118:7845-6.
24. Desobois A, Momenteau M. Lutz M. Resonance Raman spectroscopy of iron(II) super structured porphyrins: Influence of porphyrin distortion on CO and O_2 ligand dissociation. Inorg Chem 1989;28:825-34.

Microvascular responses to hemodilution with Hb vesicles as red blood cell substitutes: influence of O_2 affinity

HIROMI SAKAI,[1,2] AMY G. TSAI,[1] RONALD J. ROHLFS,[1] HIROYUKI HARA,[1,2]
SHINJI TAKEOKA,[2] EISHUN TSUCHIDA,[2] AND MARCOS INTAGLIETTA[1]
[1]*Departments of Bioengineering and Medicine, University of California, San Diego, La Jolla, California, 92093-0412; and* [2]*Department of Polymer Chemistry, Advanced Research Institute for Science and Engineering, Waseda University, Tokyo 169-8555, Japan*

Sakai, Hiromi, Amy G. Tsai, Ronald J. Rohlfs, Hiroyuki Hara, Shinji Takeoka, Eishun Tsuchida, and Marcos Intaglietta. Microvascular responses to hemodilution with Hb vesicles as red blood cell substitutes: influence of O_2 affinity. *Am. J. Physiol.* 276 (*Heart Circ. Physiol.* 45): H553–H562, 1999.—Phospholipid vesicles encapsulating purified hemoglobin (HbV) were developed to provide O_2-carrying capacity to plasma expanders. Microvascular perfusion was determined for HbV with different O_2 affinity (P_{50} = 9, 16, and 30 mmHg) prepared by coencapsulating pyridoxal 5′-phosphate (PLP) at the molar ratios of [PLP]/[Hb] = 0, 0.5, and 3, respectively (cf. hamster blood, P_{50}: 28 mmHg), and suspended in 8 g/dl human serum albumin (HSA). Eighty percent of the red blood cell (RBC) mass of conscious Syrian golden hamsters fitted with dorsal skinfold windows was substituted with either of the HbV-HSA suspensions, washed hamster RBC suspended in HSA (RBC-HSA), and HSA alone. All three HbV-HSA groups and RBC-HSA groups showed stable blood pressure and heart rate, which could not be sustained with HSA alone. Only the HbV (P_{50} = 9)-HSA group showed an increase in arterial O_2 tension (89.8 ± 14.7 mmHg, baseline 58.4 ± 4.0 mmHg) because of hyperventilation, and microvascular perfusion was decreased, indicating that facilitated O_2 unloading of HbV by decreasing the O_2 affinity (increasing P_{50}) with PLP as an allosteric effector is important. Microvascular perfusion and microvascular and interstitial O_2 tensions in the HbV (P_{50} = 16 and 30)-HSA groups were significantly higher than those in the HSA group. The O_2 release rate from the HbV was 18–32 s^{-1} vs. 4.4 s^{-1} for RBC. Functional capillary density was improved from 17 to 41% on average by decreasing P_{50} from 30 to 16 mmHg, which appears to be an optimal value for the P_{50} in this system.

oxygen carrier; microcirculation; liposome; oxygen dissociation curve; autoregulation

PHOSPHOLIPID VESICLES encapsulating concentrated hemoglobin (Hb vesicles, HbV) have the potential of becoming industrially produced red blood cell (RBC) substitutes. They most closely reproduce the characteristics of natural blood, including the RBC membrane function, by physically preventing direct contact of Hb with the cellular components of circulation (3, 19–21, 23, 24, 33). The desirability of this barrier function is evident in considering the side effects found in the use of acellular Hb solutions such as chemically modified Hb and recombinant Hb, which are now in clinical trials (34). Hb encapsulation potentially shields the microcirculation from the biological activity or toxicity of Hb and Hb-related products such as methemoglobin (metHb) and released heme. The principal systemic side effect consistently reported in the administration of acellular Hb solutions is a pressor response that has been attributed to the nitric oxide-scavenging effect of Hb due to the intrinsic high affinity of nitric oxide to Hb, a process presumed to lead to vasoconstriction (11, 18, 26). Conversely, nitric oxide-related vasoconstriction by HbV has not been observed (19).

O_2 affinity of blood is a crucial factor in determining O_2 delivery and unloading to tissues. There have been numerous theoretical analyses on the relationship between the modification of O_2 affinity (P_{50}) of RBC and resulting hemodynamic changes. Shifting the O_2 dissociation curve to the right (higher P_{50}) facilitates O_2 unloading to the tissue, reduces cardiac output, and increases vascular resistance in the absence of changes in O_2 consumption or blood pressure (15, 29). On the other hand, shifting the O_2 dissociation curve to the left (lower P_{50}) is advantageous only during severe hypoxia, because the O_2 delivery to tissues is enhanced (6, 27, 27a, 30, 35).

In terms of RBC substitutes, it has been assumed that their O_2 affinity should be the same or lower than that of blood to increase the arteriovenous difference in O_2 saturation and facilitate O_2 unloading. The relationship between the O_2 affinity of RBC substitutes and systemic or microvascular perfusion has not been presently reported. The O_2 affinity of HbV can be controlled (P_{50} = 5–150 mmHg) by selecting the appropriate amount of coencapsulated allosteric effector [pyridoxal 5′-phosphate (PLP), inositol hexaphosphate, Cl^-, H^+, etc.] without changing other physical properties (33). We prepared three kinds of HbV suspended in 8 g/dl human serum albumin (HSA) solution with different P_{50} values (9, 16, and 30 mmHg) and evaluated the effect on subcutaneous microvascular responses to severe hemodilution using conscious hamsters fitted with a dorsal skinfold chamber (8, 9, 12, 13, 24).

MATERIALS AND METHODS

Preparation of Hb vesicles with different O_2 affinities. HbVs were prepared as previously reported in the literature (21, 23). The encapsulated hemoglobin (38 g/dl) contained PLP as an allosteric effector. The inner concentrations of PLP were 0, 6, and 18 mM for the P_{50} of 9, 16, and 30 mmHg, respectively. The surface of HbV was modified with polyethyleneglycol (PEG, mol wt = 5,000) by mixing the HbV suspension with a saline solution of 1,2-dipalmitoyl-*sn*-glycero-3-

The costs of publication of this article were defrayed in part by the payment of page charges. The article must therefore be hereby marked "*advertisement*" in accordance with 18 U.S.C. Section 1734 solely to indicate this fact.

phosphatidylethanolamine-*N*-(polyethyleneglycol). HbV was ultracentrifuged and redispersed in a 8 g/dl HSA solution prepared from albumin-25% (Bayer, Germany) and saline. In our previous study, HbV was suspended in 5 g/dl HSA (24); however, we changed to 8 g/dl HSA because it showed better microvascular perfusion (i.e., increased RBC velocity and functional capillary density) than 5 g/dl HSA. The suspension was then filtered through sterilizable filters (pore size: 0.45 μm), and the Hb concentration was regulated to 10 g/dl using the HSA solution to obtain HbV-HSA suspensions with different P_{50} values. The characteristics of PEG-modified HbV-HSA suspensions are listed in Table 1, with all parameters being almost identical except for O_2 affinity.

Measurements of O_2 affinity and rate of O_2 release from HbV. O_2 affinity (P_{50}) and the Hill number of each HbV and RBC were calculated from O_2 dissociation curves measured with a Hemox Analyzer (TCS-Medical Products) at 37°C. The kinetics of O_2 release from HbV were measured by conventional rapid mixing techniques using a stopped-flow spectrophotometer (model 17 MV, Applied Photophysics, London, UK). Suspensions of air-equilibrated HbV were mixed against anaerobic solutions of dithionate, and the conversion of oxyhemoglobin to deoxyhemoglobin was monitored by the absorbance changes at 415 and 436 nm. HbV samples suspended in aerobic 50 mM phosphate-buffered saline (pH 7.4, room temperature) and 50 mM sodium dithionite were dissolved in anaerobic 50 mM phosphate-buffered saline (31). Sodium dithionite reacts with O_2 to diminish the dissolved O_2, thus HbO_2 converts to deoxyhemoglobin. The absorption decrease at 415 nm and the increase at 436 nm were monitored during deoxygenation. Four curves were obtained for each wavelength, and the rates were averaged.

Preparation of washed hamster RBC suspended in HSA. Hamster RBC suspended in HSA (RBC-HSA) were used as a reference to compare the effectiveness of HbV and to demonstrate the influence of the exchange transfusion procedure. Syrian golden hamsters (body weight of 140–150 g) were anesthetized with pentobarbital sodium (100 mg/kg body wt). A polyethylene catheter (PE-10) was implanted in the carotid artery, and blood was withdrawn with heparinized syringes, while 8 g/dl HSA solution was infused alternately by exchange transfusion. The collected blood was centrifuged to obtain an RBC concentrate. This concentrate was washed twice to remove plasma components and buffy coat by redispersion in HSA and centrifugation at 3,000 *g* for 3.5 min. The Hb concentration was adjusted to 10 g/dl, which was equivalent to the concentration of HbV-HSA.

Table 1. *Characteristics of polyethyleneglycol-modified HbVs suspended in 8% HSA with different oxygen affinity*

	HbV (P_{50}, mmHg)			Hamster RBC/HSA (P_{50}; 28 mmHg)
	9	16	30	
Diameter,[a] nm	276 ± 75	261 ± 87	253 ± 83	8,000
[Hb], g/dl	10	10	10	10
[Hb]/[lipid], g/g	1.9	1.7	1.7	
[PLP]/[Hb], mol/mol	0	0.5	3	
Hill number	1.6	1.3	2.0	2.8
OTE: 100 – 40 mmHg,[b] %	5	16	32	24
OTE: 60 – 30 mmHg,[c] %	8	19	35	31
[metHb], %	2.1	1.8	2.4	
oncotic pressure,[d] mmHg	39	39	39	39
O_2 capacity,[e] ml/100 ml	12.1	12.1	12.1	14.3

Hb, hemoglobin; HbV, vesicles encapsulating Hb; RBC, red blood cells; HSA, human serum albumin; PLP, pyridoxal 5′-phosphate; OTE, oxygen transport efficiency; metHb, methemoglobin. [a]Measured with a Coulter particle analyzer for HbVs; [b,c]difference in O_2 saturation of Hb between the indicated O_2 tensions ([b]human arteriovenous difference; [c]hamster arteriovenous difference); [d]measured with 4420 Wescor colloid osmometer (cut-off mol wt 30,000, 37°C); [e]measured with LexO_2con (Hospex, MA) fuel cell.

Animal model and preparation. Experiments were carried out in 50 male Syrian golden hamsters of 72 ± 8 g body wt (Simonsen, Gilroy, CA). With each rat under intraperitoneal pentobarbital sodium anesthesia (100 mg/kg body wt), the dorsal skinfold consisting of two layers of skin and muscle was fitted with two titanium frames with a 15-mm circular opening and surgically installed (12, 13, 24). Layers of skin muscle were separated from the subcutaneous tissue and removed until a thin monolayer of muscle and one layer of intact skin remained. A cover glass (diameter, 12 mm) was held by one frame on the exposed tissue allowing intravital observation of the microvasculature and tissues.

Polyethylene tubes (PE-10, 1 cm), which were connected to PE-50 (25 cm) via silicone elastomer medical tubes (4 cm, Technical Products), were implanted in the jugular vein and the carotid artery. They were passed from the ventral to the dorsal side of the neck and exteriorized through the skin at the base of the chamber. Patency of the catheters was ensured by filling with heparinized saline (40 IU/ml).

Microvascular observations of the awake and unanesthetized hamsters were performed at least 3 days after chamber implantation to mitigate postsurgical trauma. We used conscious hamsters because anesthesia alters microvascular perfusion, which depends on the deepness of anesthesia (12). During the measurements, the animals were placed in a perforated plastic tube (inner diameter, 3.8 cm; length, 17 cm), from which the window chamber protrudes, to minimize animal movement without impeding respiration.

A preparation was considered suitable for experimentation if microscopic examination of the window chamber met the following criteria: *1*) no sign of bleeding and/or edema; *2*) systemic mean arterial pressure (MAP) was >80 mmHg; and *3*) heart rate was above 320 beats/min.

All animal studies were approved by the Animal Subject Committee of University of California, San Diego, and the National Institutes of Health *Guide for the Care and Use of Laboratory Animals* [DHHS Publication No. (NIH) 85-23, Revised 1985] principles have been observed.

Experimental procedure. Isovolemic hemodilution with the experimental fluids was performed by the simultaneous withdrawal of blood from the arterial catheter and infusion of the test substitutes into the venous catheter at a rate of 0.3 ml/min as described previously (24).

Microhemodynamic and systemic parameters were evaluated at 0, 30, 60, and 80% levels of exchange. Thirty-three hamsters were exchange transfused in five groups with PEG-modified HbV-HSA with P_{50} = 9 mmHg (n = 6), 16 mmHg (n = 7), and 30 mmHg (n = 7), and washed hamster RBC-HSA (n = 6), and HSA alone (n = 7). The in situ microcirculation of the skinfold chamber was observed using a video-microscope system. After the blood substitution, a bolus intravenous injection of palladium-porphyrin bound to bovine albumin solution (7.6 wt%, 0.1 ml) was injected to measure the O_2 tensions (Po_2) in vessels and interstitium (12, 13) (see *Determination of microvascular and interstitial O_2 tensions).* Seventeen hamsters were used for baseline Po_2 measurement.

Microhemodynamic analysis. Microvessels in the subcutaneous tissue and the skeletal skin muscle were observed with an inverted microscope and by the transillumination technique. Microvessels were classified according to their position within the microvascular network. Arteriolar microvessels were grouped into large feeding arterioles (A_1; diameter, 57 ±

14 μm), small arcading arterioles (A_2, 25 ± 8 μm), transverse arterioles (A_3, 10 ± 2 μm), and terminal arterioles (A_4, 9 ± 2 μm). Venules were classified as small collecting venules (V_C, 28 ± 6 μm) and large venules (V_L, 80 ± 15 μm). The microvessels selected for measurements were chosen for their optical clarity and not by the nature of the flow. Capillaries and tissue segments selected for measurements were supplied and drained by the arterioles and venules of a functional microvascular unit. These microvessels and capillaries were sketched in advance to plan the sequence of measurements.

Microvascular diameter and RBC velocity were analyzed on-line in arterioles and venules (8, 24). Vessel diameter was measured with an image-shearing system, whereas RBC velocity was analyzed by photodiodes and the cross-correlation technique. Blood flow rates ($\dot{Q}$) were calculated using the equation

$$\dot{Q} = (\text{RBC velocity}/R_v)\cdot\pi\cdot(\text{diameter}/2)^2 \quad (1)$$

where R_v represents the ratio of velocity in the middle of vessels to whole blood velocity based on the data in the glass tubes. R_v at 1.6 was used for A_1, A_2, V_C, and V_L, and R_v at 1.3 was used for A_3 and A_4.

Functional capillary density was analyzed on-line by counting the number of capillaries with RBC flow stemming from one A_3 arteriole, usually 40–80 capillaries, and expressed as a percentage of the basal value.

Characterization of systemic conditions. Blood samples were collected in heparinized microtubes for the hematocrit and blood gas analyses. A pH/blood gas analyzer (Ciba Corning 238, Ciba Corning Diagnostic, Pleasanton, CA) was used for analysis of arterial blood O_2 tension (Pa_{O_2}), arterial blood carbon dioxide tension (Pa_{CO_2}), pH, and base excess. An analogue recording system (Beckman R611, Beckman Instruments, Schiller Park, IL) was used for continuous monitoring of MAP and heart rate.

Determination of microvascular and interstitial O_2 tensions. Subcutaneous microvascular and interstitial P_{O_2} were determined with the O_2-dependent quenching of phosphorescence emitted by palladium-*meso*-tetra(4-carboxyphenyl)porphyrin bound to serum albumin after pulsed light excitation (8, 9, 12, 13). The method allows noninvasive assessment of intravascular P_{O_2} and determination of interstitial oxygenation, because intravascularly injected porphyrin-albumin complexes extravasate into the interstitium over time. P_{O_2} can be obtained using the Stern-Volmer equation from the phosphorescence lifetimes.

Percentage of microvascular O_2 consumption after 80% level of exchange ($\dot{V}_{mO_2}$) in comparison with baseline was calculated using the equation

$$\dot{V}_{mO_2} = \frac{\dot{Q}_{av} \times \{[Hb]_{RBC} \times (S_{A_1}O_2 - S_{V_L}O_2) + [Hb]_{HbV} \times (S'_{A_1}O_2 - S'_{V_L}O_2)\}}{14 \times 18} \quad (2)$$

where $\dot{Q}_{av}$ is the averaged percentage of blood flows in A_1 and V_L relative to baseline. $[Hb]_{RBC}$ and $[Hb]_{HbV}$ are Hb concentrations of RBC and HbV, respectively, which were estimated from the hematocrit. $S_{A_1}O_2$ and $S'_{A_1}O_2$ are O_2 saturations in A_1 of RBC and HbV, respectively, and $S_{V_L}O_2$ and $S'_{V_L}O_2$ are those in V_L. They were estimated from the O_2 dissociation curves of HbVs and RBC in Fig. 1 and microvascular O_2 tensions. The initial Hb concentration and arteriovenous difference in the microvasculature ($S_{A_1}O_2 - S_{V_L}O_2$) before the blood exchange were estimated to be 14 g/dl and 18%, respectively.

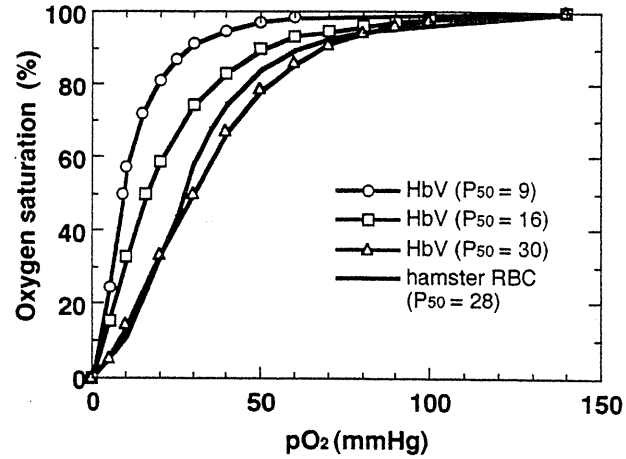

Fig. 1. O_2 dissociation curves of 3 hemoglobin vesicles (HbV) with different O_2 affinities measured with an Hemox analyzer at 37°C and hamster red blood cells (RBC) cited from Stein and Ellsworth (27a).

Data analysis. Data were analyzed using ANOVA followed by Fisher's protected least significant difference test between the groups. Paired *t*-test was used for the time-dependent comparisons with the baseline values in each group. The level of confidence was placed at 95% for all the experiments.

RESULTS

O_2 affinities and O_2 release rates of HbV. The value of P_{50} (P_{O_2} at which Hb saturates with half O_2) of HbV without PLP as an allosteric effector showed 9 mmHg, and it increased to 16 and 30 mmHg by coencapsulating PLP at the ratios of PLP/Hb = 0.5 and 3, respectively (Fig. 1). O_2 transport efficiencies (OTE; difference in O_2 saturation between arterial and venous O_2 tension) were 5, 16, and 32%, when calculated using the human arteriovenous difference at P_{50} = 9, 16, and 30 mmHg, respectively, and 4, 19, and 36%, respectively, when calculated using the hamster arteriovenous difference. Even though the P_{50} of HbV (P_{50} = 30) was close to that of hamster RBC (28 mmHg), its Hill number (indicator of subunits cooperativity) was smaller than that of hamster RBC. Therefore, the slope of HbV (P_{50} = 30) is steeper at a P_{O_2} of 60 mmHg, and the trend reverses at ~30 mmHg.

The rates of O_2 release of three HbVs in the presence of excess sodium dithionite in the outer media were 18, 27, and 32 s^{-1} at P_{50} = 9, 16, and 30 mmHg, respectively (Fig. 2). These rates were much slower than the rate of purified small arteries (HbA_o; 84 s^{-1}). However, these are much faster than RBC (2.0–9.1 s^{-1}) reported by Vandegriff and Olson (31).

Changes in systemic parameters during hemodilution. Hematocrit before the exchange transfusion was 47–50% on the average, and it was reduced to ~7% after 80% level of exchange for all the groups except the RBC-HSA group, which was 31% (Table 2). This was due to the infusion of RBC suspension with a hematocrit of ~30%. The actual levels of blood exchange calculated from the hematocrit were ~32, 64, and 85% for the theoretical values of 30, 60, and 80%, respectively.

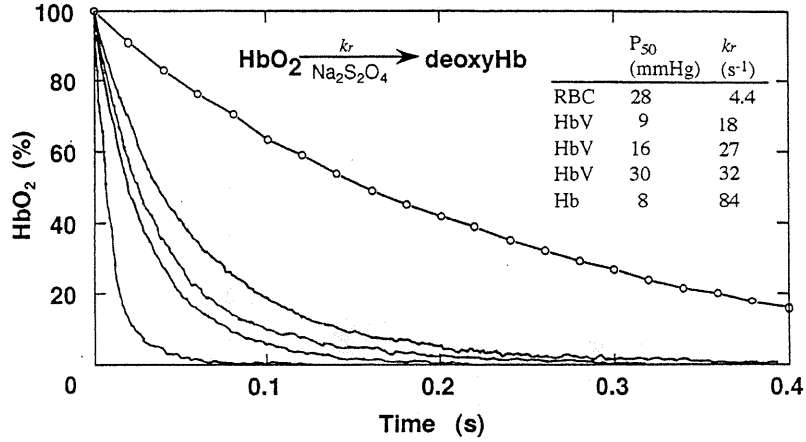

Fig. 2. Time courses of O_2 release by RBC, HbVs, and HbA_o, measured with a stopped flow method, mixing an air-equilibrated Hb containing sample (10 μM) and deoxygenated sodium dithionate solution (50 mM), room tempertature, in 50 mM phosphate-buffered saline (pH 7.4). *Inset*, from *top* to *bottom*: RBC, HbV (P_{50} = 9, 16, and 30 mmHg) and HbA_o. Curve of human RBC was cited from Vandegriff and Olson (31). k_r, O_2 release rate.

The HSA and HbV (P_{50} = 9)-HSA groups had increased Pa_{O_2}. The HSA group showed a dramatic change from 61.6 ± 9.4 mmHg as baseline to 117.3 ± 4.6 mmHg. The HbV (P_{50} = 9)-HSA group increased from 58.4 ± 4.0 mmHg to 89.8 ± 14.7 mmHg. However, the other two groups HbV (P_{50} = 16 and 30)-HSA groups showed stable values, and they were significantly lower than the others.

The HSA and HbV (P_{50} = 9)-HSA groups showed a significant drop in Pa_{CO_2} from 56.0 ± 3.2 and 60.3 ± 4.0 mmHg at baseline to 37.6 ± 7.1 and 47.2 ± 11.0 mmHg at 80% level of exchange, respectively. The other three groups, HbV (P_{50} = 16 and 30)-HSA, and RBC/HSA had stable values that were significantly higher than the HSA group.

The HSA group exhibited a significant increase in pH from 7.390 ± 0.029 at baseline to 7.448 ± 0.069 at 80% level of exchange because of respiratory alkalosis. The RBC-HSA group also showed a drop in pH, whereas it was significantly higher than the HSA group.

The HSA group showed a significant drop in base excess to −1.65 ± 0.21 mmol/l (baseline, 5.10 ± 0.85

Table 2. *Systemic hematocrit and blood gas parameters during hemodilution with HSA, HbV/HSAs, or hamster RBC/HSA*

Group	Level of Blood Exchange, %			
	Baseline	30	60	80
Systemic hematocrit %				
HSA	49.1 ± 2.3	31.5 ± 1.0*	17.0 ± 0.9*	7.5 ± 1.1*
HbV (P_{50} = 9)-HSA	48.9 ± 2.7	33.4 ± 1.5*	17.6 ± 1.0*	7.1 ± 1.3*
HbV (P_{50} = 16)-HSA	48.2 ± 2.6	32.3 ± 1.1*	17.3 ± 1.4*	6.9 ± 0.6*
HbV (P_{50} = 30)-HSA	50.4 ± 1.6	33.1 ± 1.0*	17.2 ± 1.0*	7.4 ± 1.1*
RBC-HSA	47.6 ± 2.4	40.2 ± 2.1*†	33.4 ± 3.2*†	31.0 ± 2.0*†
Pa_{O_2}, mmHg				
HSA	61.6 ± 9.4	69.2 ± 7.7*	87.1 ± 12.4*	117.3 ± 4.6*
HbV (P_{50} = 9)-HSA	58.4 ± 4.0	65.1 ± 6.8*	74.7 ± 15.1*†	89.8 ± 14.7*
HbV (P_{50} = 16)-HSA	60.7 ± 6.8	63.2 ± 5.0†	65.0 ± 7.6†	63.2 ± 9.2†
HbV (P_{50} = 30)-HSA	59.2 ± 5.0	57.4 ± 7.2†	61.9 ± 6.0†	58.2 ± 5.5†
RBC/HSA	60.4 ± 4.7	65.4 ± 5.9	69.6 ± 7.7*†	68.0 ± 8.4†
Pa_{CO_2}, mmHg				
HSA	56.0 ± 3.2	54.1 ± 4.3	50.4 ± 7.3*	37.6 ± 7.1*
HbV (P_{50} = 9)-HSA	60.3 ± 4.0	57.5 ± 6.6	54.9 ± 10.2	47.2 ± 11.0*†
HbV (P_{50} = 16)-HSA	62.6 ± 2.8	61.8 ± 4.8†	57.7 ± 5.5*†	56.6 ± 6.7*†
HbV (P_{50} = 30)-HSA	61.0 ± 1.9	58.9 ± 2.7	56.6 ± 5.3*	57.9 ± 3.5†
RBC-HSA	57.1 ± 7.7	55.4 ± 9.0	54.1 ± 7.1	50.8 ± 4.6†
pH				
HSA	7.390 ± 0.029	7.403 ± 0.019	7.462 ± 0.030*	7.448 ± 0.069
HbV (P_{50} = 9)-HSA	7.380 ± 0.013	7.388 ± 0.038	7.373 ± 0.053†	7.394 ± 0.082
HbV (P_{50} = 16)-HSA	7.341 ± 0.023	7.340 ± 0.037	7.336 ± 0.032†	7.306 ± 0.046†
HbV (P_{50} = 30)-HSA	7.362 ± 0.043	7.364 ± 0.046	7.343 ± 0.026†	7.323 ± 0.045†
RBC/HSA	7.392 ± 0.030	7.386 ± 0.028	7.403 ± 0.021†	7.401 ± 0.019
Base excess, mmol/l				
HSA	5.10 ± 0.85	5.20 ± 1.13	5.90 ± 3.39	−1.65 ± 0.21*
HbV (P_{50} = 9)-HSA	7.52 ± 2.40	6.75 ± 1.95*	4.23 ± 2.91*	2.15 ± 3.45*
HbV (P_{50} = 16)-HSA	7.20 ± 2.10	6.81 ± 1.66	4.57 ± 1.77*	1.38 ± 1.56*
HbV (P_{50} = 30)-HSA	8.24 ± 3.87	7.30 ± 3.69	4.40 ± 3.23*	3.23 ± 2.86*†
RBC-HSA	8.30 ± 1.24	6.68 ± 2.44	6.70 ± 1.30*	5.03 ± 2.18*†

Values are means ± SD. * Significant difference from baseline ($P < 0.05$); † significant difference from the HSA group ($P < 0.05$). Pa_{O_2}, arterial blood oxygen tension; Pa_{CO_2}, arterial blood carbon dioxide tension.

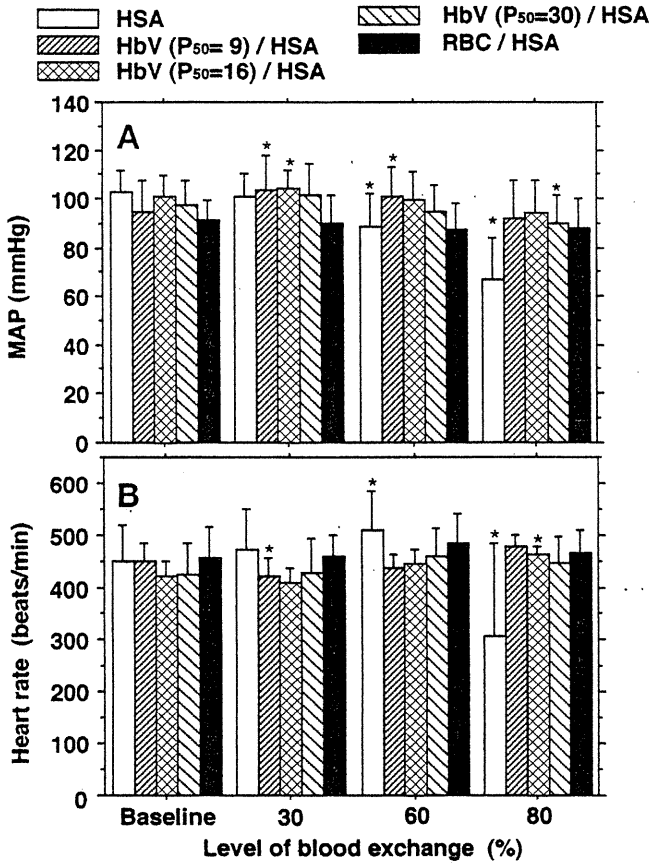

Fig. 3. Changes in mean arterial pressure (MAP; *A*) and heart rate (*B*) during hemodilution with HbV-human serum albumin (HSA), HSA, and washed RBC-HSA. Values are means ± SD. * Significantly different from baseline ($P < 0.05$).

mmol/l), indicating severe anemia. The other four groups also showed the drops in base excess, whereas they were significantly higher than the HSA group.

As for the systemic hemodynamics, all the HbV-HSA groups showed slight increases in MAP (Fig. 3). The HSA group started to show a significant decrease at 60% level of exchange and dropped to 66.8 ± 17.1 mmHg (baseline, 103.0 ± 8.3 mmHg) at 80% exchange. The other four groups receiving O_2-carrying fluids showed higher values that were stable even after the completion of the blood exchange.

Heart rate of all the groups maintained the normal values except the HSA group, which showed an increase to 509 ± 74 beats/min at 60% level of exchange and then a decrease to 309 ± 174 beats/min at 80% level of exchange (baseline, 448 ± 69 beats/min) because of cardiovascular insufficiency consequent to anemia.

Microhemodynamic responses to hemodilution. Basal values for the microvessel diameters and blood flow rates are shown in Table 3. There is no significant difference between the groups.

Venules of the HSA group constricted up to the 80% level of exchange (V_L, −26% on the average in comparison with baseline; V_C, −7%) (Fig. 4), whereas the arterioles tended to dilate. These phenomena may be related to blood redistribution from the skin to the vital organs as anemia progressed. The RBC-HSA group showed some diameter changes, but they were not consistent. The three HbV-HSA groups showed rather stable values.

The HSA group showed higher rates of blood flow in comparison with baseline in A_2 (+9%) and A_3 (+33%) at 30% level of exchange and in A_1 (+18%), A_3 (+17%), and A_4 (+40%) at 60% level of exchange (Fig. 5). This is a typical phenomenon for hemodilution with plasma expanders (17). However, the HSA group had a significant drop to nearly zero at the final exchange. The other four groups showed significantly higher rates of blood flow at 80% level of exchange. The RBC-HSA group maintained the flow rates in A_1, A_2, and V_L and showed significantly higher rates at 60% level of exchange in V_C (+91%). The HbV-HSA groups showed lower values than the RBC-HSA group; however, the HbV (P_{50} = 16)-HSA group showed nonsignificantly the highest values among the three in A_1, A_2, A_3, V_C, and V_L. Flow in the HbV (P_{50} = 9)-HSA group dropped significantly at the first 30% level of exchange and maintained the lowest value among the three.

Functional capillary density of the RBC-HSA group was maintained at the highest value throughout the hemodilution (80 ± 28% at 80% level of exchange) (Fig. 6). The HSA group maintained high values up to the 60% level of exchange; however, it dropped to 1.4 ± 2.3% at the final exchange. The three HbV-HSA groups showed significantly lower values than the RBC-HSA

Table 3. *Basal values for the diameters and blood flow rates of arterioles and venules*

Group	A_1	A_2	A_3	A_4	V_C	V_L
Diameter, μm						
HSA	57.1 ± 12.6	24.0 ± 9.7	8.7 ± 1.9	8.7 ± 1.9	25.5 ± 1.7	79.9 ± 21.4
HbV (P_{50} = 9)-HSA	61.0 ± 13.5	22.9 ± 8.6	10.6 ± 2.0	10.1 ± 2.5	32.9 ± 2.9	83.3 ± 6.2
HbV (P_{50} = 16)-HSA	52.1 ± 15.6	23.4 ± 2.8	10.7 ± 2.6	10.0 ± 1.8	28.4 ± 8.3	83.6 ± 16.8
HbV (P_{50} = 30)-HSA	56.7 ± 15.7	28.2 ± 5.1	10.6 ± 1.4	9.0 ± 1.2	27.4 ± 7.0	82.0 ± 16.4
RBC/HSA	59.7 ± 14.5	24.1 ± 4.3	9.1 ± 0.9	8.3 ± 2.0	25.3 ± 4.2	74.4 ± 14.8
Blood flow rate, nl/s						
HSA	24.3 ± 24.3	3.8 ± 4.5	0.20 ± 0.20	0.14 ± 0.09	0.39 ± 0.17	12.6 ± 7.9
HbV (P_{50} = 9)-HSA	17.7 ± 15.6	1.8 ± 0.7	0.24 ± 0.22	0.20 ± 0.22	0.39 ± 0.08	12.6 ± 3.2
HbV (P_{50} = 16)-HSA	8.3 ± 7.9	1.4 ± 0.9	0.25 ± 0.25	0.15 ± 0.17	0.40 ± 0.25	12.8 ± 7.2
HbV (P_{50} = 30)-HSA	15.3 ± 14.3	2.0 ± 1.5	0.16 ± 0.53	0.10 ± 0.06	0.34 ± 0.34	8.1 ± 4.7
RBC-HSA	19.9 ± 13.0	2.3 ± 1.6	0.18 ± 0.10	0.12 ± 0.11	0.36 ± 0.25	8.2 ± 7.3

Values are means ± SD. A_1–A_4, arterioles; V_C and V_L, collecting and large venules.

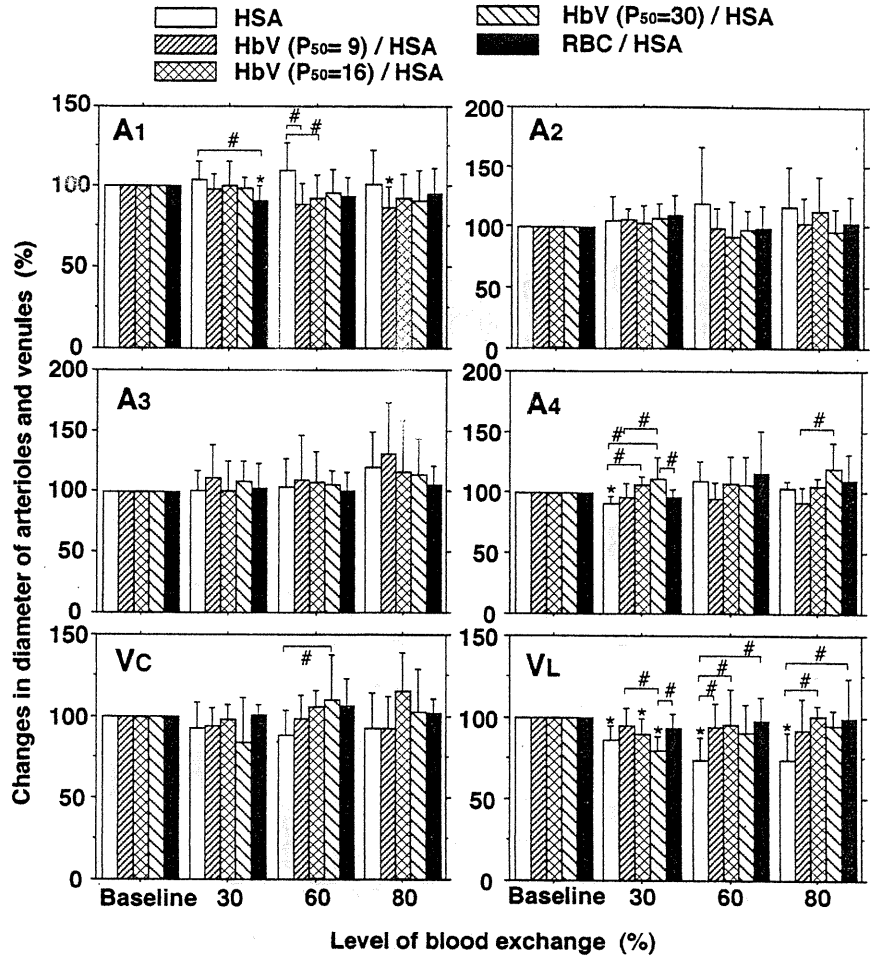

Fig. 4. Diameter changes of arterioles (A_1–A_4) and collecting and large venules (V_C and V_L, respectively) of skinfold preparation during hemodilution. Values are means ± SD. *Significantly different from baseline ($P < 0.05$); # significantly different between indicated groups ($P < 0.05$).

group; however, they were all higher than the HSA group at the 80% level of exchange. The HbV (P_{50} = 16)-HSA group showed the highest density among the three. Because functional capillary density was measured by counting the number of capillaries where there was flow of RBCs, the values for the HSA and HbV-HSA groups might be underestimated because of plasma skimming.

Microvascular and interstitial O_2 tensions. Normally A_1 had 51.1 ± 6.3 mmHg in P_{O_2}, decreasing to 39.3 ± 4.8 mmHg in A_4 arterioles (Fig. 7). This reduction is associated with the diffusion of O_2 from these arterioles (4, 9, 28). After perfusion through the capillaries, the P_{O_2} in venules increased from 33.8 ± 9.8 mmHg in V_C to 35.6 ± 5.8 mmHg in V_L because of the presence of the O_2 shunt. The P_{O_2} values of the HSA group were consistently very low (<23.9 ± 9.7 mmHg). The other four groups maintained significantly higher values than the HSA group, and the RBC-HSA group had P_{O_2} values that were close to baseline. The three HbV-HSA groups were lower than the RBC-HSA group; however, the HbV (P_{50} = 16 and 30)-HSA groups showed significantly higher values than the HbV (P_{50} = 9)-HSA group in A_1, A_2, and A_4. Interstitial P_{O_2} is slightly higher for HbV (P_{50} = 16)-HSA than HbV (P_{50} = 30)-HSA.

Relative microvascular O_2 consumption. Relative O_2 consumption in the microvasculature after exchange ($\dot{V}_{mO_2}$) in comparison with the baseline can be estimated from the change in blood flow, Hb concentration, and arteriovenous (A_1-V_L) difference. As shown in Fig. 8, the HSA group showed 7.4% of $\dot{V}_{mO_2}$ relative to baseline. Other groups showed significantly higher values than the HSA group, although the HbV (P_{50} = 9)-HSA group showed significantly lower $\dot{V}_{mO_2}$ than the baseline (19.0%). The RBC-HSA group maintained the highest level of $\dot{V}_{mO_2}$ (101.0%). The HbV (P_{50} = 16 and 30)-HSA groups showed almost the same values on the average (79.7 and 80.7%, respectively). They were lower than the RBC-HSA group without significant difference. The A_1-V_L differences in O_2 saturation of RBC ($S_{A_1}O_2$ − $S_{V_L}O_2$) were 37, 47, 44, 58, 30, and 18% for the groups of HSA, HbV (P_{50} = 9, 16, and 30)-HSA, RBC-HSA, and baseline, respectively. Those differences of HbV ($S'_{A_1}O_2$ − $S'_{V_L}O_2$) were 38, 32, and 51% for HbV-HSA (P_{50} = 9, 16, and 30, respectively). The HbV-HSA (P_{50} = 30) showed the highest A_1-V_L differences in O_2 saturation for both RBC and HbV.

DISCUSSION

Our results show that all three HbV-HSA groups with different P_{50} values showed similar stable systemic hemodynamics during severe hemodilution, which could not be sustained by HSA alone; however, there

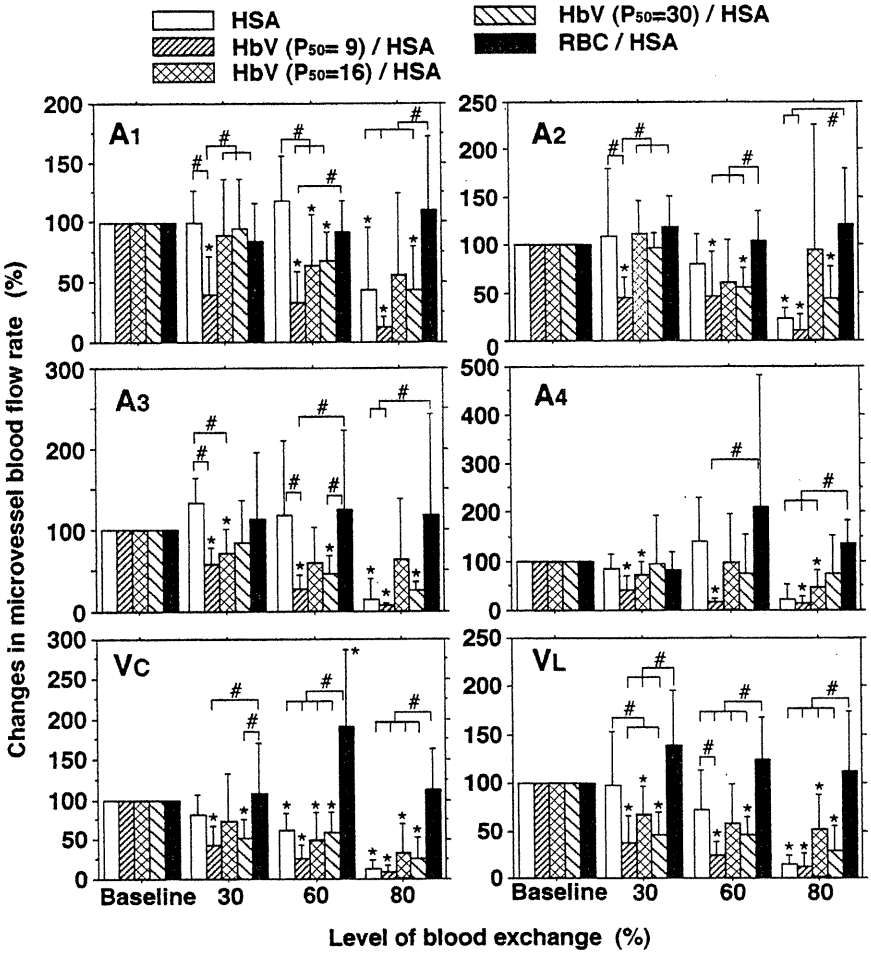

Fig. 5. Changes in flow rates in arterioles (A_1–A_4) and venules (V_C and V_L) of skinfold preparation during hemodilution. Values are means ± SD. *Significantly different from baseline ($P < 0.05$); #significantly different between indicated groups ($P < 0.05$).

were significant differences in blood gas and microhemodynamic parameters. This becomes apparent when severe hemodilution is performed to hematocrit <10%. This level of blood exchange is necessary for a testing of RBC substitutes in terms of safety and efficacy (1, 3, 24), because an exchange of up to 60% with non-O_2-carrying HSA does not show significant differences from normal microhemodynamic parameters. Among the three HbV groups, HbV (P_{50} = 16 and 30)-HSA showed significantly improved microvascular perfusion than the HbV (P_{50} = 9)-HSA, which emphasizes the importance of facilitated O_2 unloading of HbV by decreasing the O_2 affinity with PLP as an allosteric effector. Although the HbV (P_{50} = 9)-HSA group maintained stable blood pressure and heart rate, the increase in Pa_{O_2} was remarkable. This is due to hyperventilation, suggesting the decreased O_2 off-loading from the HbV with high O_2 affinity. Arteriovenous difference was increased by the lowered O_2 tension in V_L (38%; baseline, 18%); however, O_2 consumption in the subcutaneous microvasculature was diminished mainly as a consequence of the significantly decreased blood flow rates.

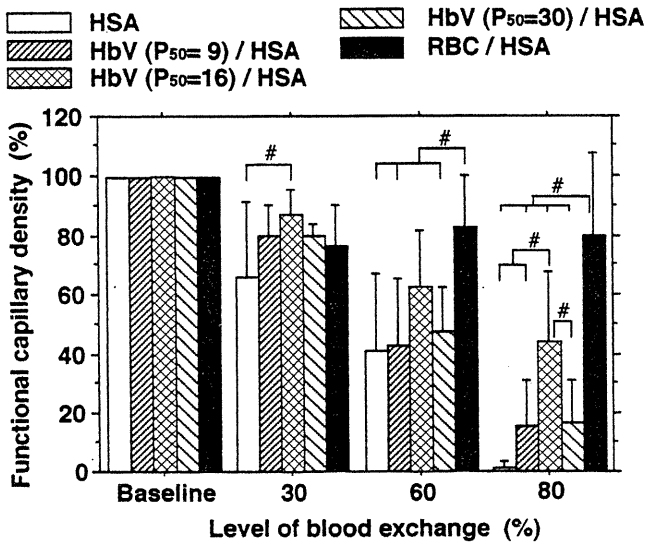

Fig. 6. Changes in functional capillary density during hemodilution. Values are means ± SD. *Significantly different from baseline ($P < 0.05$); #significantly different between indicated groups ($P < 0.05$).

The HbV (P_{50} = 16 and 30)-HSA groups maintained values comparable with the RBC-HSA group up to the 60% level of exchange, suggesting an improved O_2 supply. Even though the microvascular perfusion of the HbV (P_{50} = 16 and 30)-HSA groups were inferior to the RBC-HSA group at 80% level of exchange, the HbV (P_{50} = 16)-HSA group showed relatively higher func-

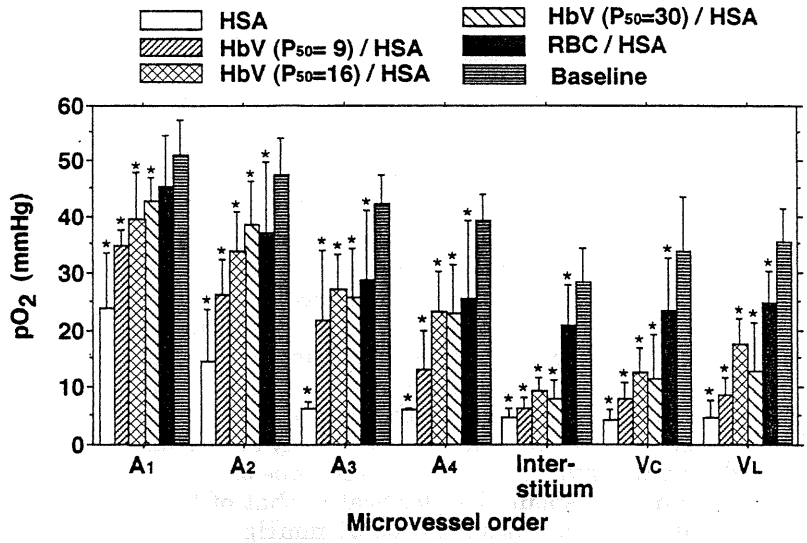

Fig. 7. O_2 tensions of microvasculature (A_1–A_4, V_C, and V_L) and interstitium after 80% exchange and baseline value. Values are means ± SD. *Significantly different from baseline ($P < 0.05$).

tional capillary density and flow rates than the $P_{50} = 30$ group. This corresponds to the result of Woodson and Auerbach (35), who found increased blood flow in the heart, brain, and spleen without changes in cardiac output and blood pressure when O_2 affinity of rat RBCs was increased to a $P_{50} = 17$ mmHg from the normally 38 mmHg. They concluded that this is a compensatory response to decreased O_2 delivery. It was shown previously in our model that most of the O_2 is diffusively supplied primarily from arterioles rather than capillaries in normal condition, as evidenced by the fall in O_2 tension from A_1 to A_4 arterioles in Fig. 7 (9). Because functional capillary density may be related to mechanisms in addition to O_2 delivery, an improvement of this parameter may lead to enhanced tissue viability.

There was not enough vasoconstriction for the HbV-HSA groups to explain the reduced blood flow rates in comparison with the RBC-HSA group. Subcutaneous blood flow is probably regulated in part at the level of microvasculature under the observation and by thoracodorsal arteries or larger arteries not visible in the preparation (22). Normally, the low O_2 solubility in plasma creates a major barrier to the diffusion of O_2 in the plasma space between RBCs and vascular walls. It has been speculated that exposure of arteries or arterioles to high O_2 tension induced autoregulatory limitation of O_2 delivery by restricting flow with decreased endothelial prostaglandin synthesis, thus increasing peripheral vascular resistance (2, 7, 10, 16). The hypothesis has been suggested that acellular RBC substitutes (Hb solution) produce a higher O_2 availability because of the homogeneously dissolved Hb, leading to a microcirculation-limited O_2 delivery due to vasoconstriction (9, 32). HbVs may have the same effect because they are much smaller than RBCs and are dispersed relatively homogeneously throughout the plasma (24). As shown in Fig. 2, O_2 release from the acellular Hbs is faster than the release from HbVs and RBCs at the same heme concentration and same O_2 affinity, because O_2 must diffuse through the viscous Hb solutions in the vesicles to the outside and through the solvent layer surrounding each HbV particle and RBC. O_2 release from the HbV is much faster than that from RBC because particle size is smaller (0.25 μm vs. 8 μm), providing a much smaller surface area-to-volume ratio for diffusion (32). This may explain the higher functional capillary densities and blood flow rates for HbV ($P_{50} = 16$)-HSA vs. HbV ($P_{50} = 30$)-HSA. However, we could not obtain better results with HbV ($P_{50} = 9$)-HSA even though its O_2 release rate is slowest and the closest to that of RBC. All known Hb-related blood substitutes appear to have faster O_2 release than HbVs ($P_{50} = 9$). Given these considerations, the amount of O_2 unloaded (arteriovenous difference or O_2 transporting efficiency) estimated from the O_2 dissociation curve may be crucial.

The different shapes of O_2 dissociation curves (Fig. 1) can also explain our observations. Even though the O_2

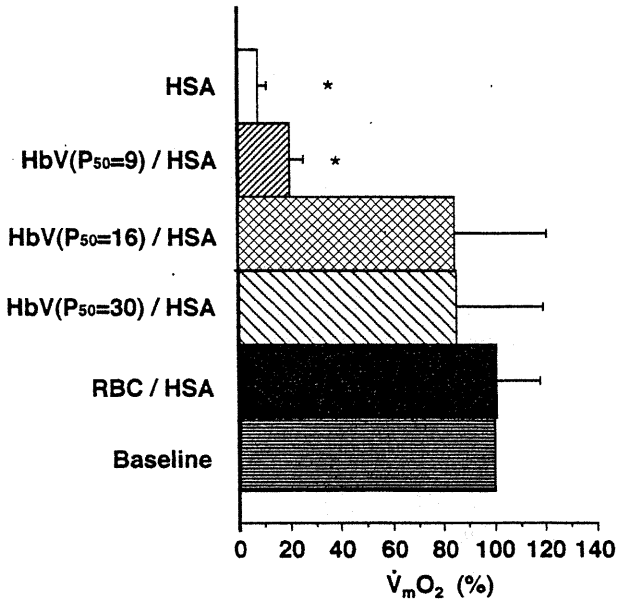

Fig. 8. Relative O_2 consumptions ($\dot{V}_{mO_2}$) of microvasculature after 80% blood exchange in comparison with baseline. Values are means ± SE. *Significantly different from baseline ($P < 0.05$).